The HARPS search for southern extra-solar planets

C. Mordasini, M. Mayor, S. Udry, C. Lovis, D. Ségransan, W. Benz, Jean-Loup Bertaux, F. Bouchy, G. Lo Curto, C. Moutou, et al.

A&A 526, A111 (2011)
DOI: 10.1051/0004-6361/200913521

Astronomy & Astrophysics

The HARPS search for southern extra-solar planets⋆,⋆⋆

XXIV. Companions to HD 85390, HD 90156, and HD 103197: a Neptune analog and two intermediate-mass planets

C. Mordasini[1,2], M. Mayor[3], S. Udry[3], C. Lovis[3], D. Ségransan[3], W. Benz[2], J.-L. Bertaux[4], F. Bouchy[5], G. Lo Curto[6], C. Moutou[7], D. Naef[3,6], F. Pepe[3], D. Queloz[3], and N. C. Santos[8]

[1] Max-Planck-Institut für Astronomie, Königstuhl 17, 69117 Heidelberg, Germany
e-mail: mordasini@mpia.de
[2] Physikalisches Institut, Universität Bern, Sidlerstrasse 5, 3012 Bern, Switzerland
[3] Observatoire de Genève, Université de Genève, 51 Ch. des Maillettes, 1290 Sauverny, Switzerland
[4] Service d'Aéronomie du CNRS/IPSL, Université de Versailles Saint-Quentin, BP 3, 91371 Verrières-le-Buisson, France
[5] Institut d'Astrophysique de Paris, CNRS, Université Pierre et Marie Curie, 98bis Bd Arago, 75014 Paris, France
[6] European Southern Observatory, Casilla 19001, Santiago 19, Chile
[7] Laboratoire d'Astrophysique de Marseille, Traverse du Siphon, 13376 Marseille Cedex 12, France
[8] Centro de Astrofísica da Universidade do Porto, Rua das Estrelas, 4150-762 Porto, Portugal

Received 21 October 2009 / Accepted 1 October 2010

ABSTRACT

We report the detection of three new extrasolar planets orbiting the solar type stars HD 85390, HD 90156 and HD 103197 with the HARPS spectrograph mounted on the ESO 3.6-m telescope at La Silla observatory. HD 85390 has a planetary companion with a projected intermediate mass (42.0 $M_\oplus$) on a 788-day orbit (a = 1.52 AU) with an eccentricity of 0.41, for which there is no analog in the solar system. A drift in the data indicates the presence of another companion on a long-period orbit, which is however not covered by our measurements. HD 90156 is orbited by a warm Neptune analog with a minimum mass of 17.98 $M_\oplus$ (1.05 M_Ψ), a period of 49.8 days (a = 0.25 AU), and an eccentricity of 0.31. HD 103197 has an intermediate-mass planet on a circular orbit (P = 47.8 d, $M \sin i$ = 31.2 $M_\oplus$). We discuss the formation of planets of intermediate mass (~30–100 $M_\oplus$), which should be rare inside a few AU according to core accretion formation models.

Key words. planetary systems – techniques: radial velocities – stars: individual: HD 85390 – stars: individual: HD 90156 – stars: individual: HD 103197 – planetary systems: formation

1. Introduction

The HARPS (high accuracy radial velocity planet searcher) program has continued since 2003 at the ESO 3.6 m telescope located at La Silla Observatory in Chile (Pepe 2002). Thanks to its high accuracy of $\lesssim$1 m/s and its long time stability, HARPS has in particular detected many low-mass planets, starting with μ Arae b at the beginning of the program (Santos et al. 2004) to the recent two Earth-mass planet around GJ 581 (Mayor et al. 2009). As such low-mass planets seem to be very abundant (Lovis et al. 2009), HARPS helps to increase the number of known extrasolar planets. This number is raising rapidly in time t, roughly as $t^{2..3}$ since the discovery of 51 Peg b by Mayor & Queloz (1995) fifteen years ago.

These detections of extrasolar planets have stimulated the research on planet formation enormously. They have shown the importance of mechanisms that were previously underestimated in their importance because of the shape of our own solar system alone, such as orbital migration, which was known on purely theoretical grounds for a long time (Goldreich & Tremaine 1980), overthrowing the idea that giant planets can only be found beyond a few astronomical units (Boss 1995).

The quickly growing number of extrasolar planets has allowed many important distributions of physical properties and orbital elements to be derived. We now know the distributions of masses, semi-major axes, or the eccentricities of giant planets within a few AU around solar-like stars (e.g. Udry & Santos 2007) and see correlations between stellar and planetary parameters. The most important example is the "metallicity effect", i.e. the increase in giant planet frequency with stellar [Fe/H], see e.g. Santos et al. (2001) or Fischer & Valenti (2005).

By varying the initial conditions of planetary formation models in a Monte Carlo way (Ida & Lin 2004), one can also try to derive these statistical distributions from theoretical formation models and compare them with the observed ones. This young method of planetary population synthesis (Mordasini et al. 2009a,b) allows the full wealth of observational data to be used to constrain theoretical models and to improve our understanding of planet formation, as demonstrated here for the specific case of intermediate-mass planets.

In this paper we report the discovery of two types of planets, one Neptunian planet and two intermediate-mass planets (about

⋆ Based on observations made with the HARPS instrument on the ESO 3.6 m telescope at La Silla Observatory under the GTO program ID 072.C-0488.

⋆⋆ Individual radial velocities are available electronically at CDS via anonymous ftp to cdsarc.u-strasbg.fr (130.79.128.5) or via http://cdsarc.u-strasbg.fr/viz-bin/qcat?J/A+A/526/A111

Table 1. Observed and inferred stellar parameters for the three host stars.

Parameter	Unit	HD 85390[†]	HD 90156[†]	HD 103197[‡]
Spectral type		K1V	G5V	K1Vp
V	[mag]	8.54	6.92	9.40
$B-V$	[mag]	0.86	0.66	0.86
π	[mas]	29.45 ± 0.84	45.26 ± 0.75	20.27 ± 1.47
M_V	[mag]	5.89	5.20	5.77
$T_{\rm eff}$	[K]	5186 ± 54	5599 ± 12	5303 ± 58
$\log g$	[cgs]	4.41 ± 0.09	4.48 ± 0.02	4.40 ± 0.11
[Fe/H]	[dex]	-0.07 ± 0.03	–0.24 ± 0.01	0.21±0.04
L	[$L_\odot$]	0.43 ± 0.03	0.72 ± 0.01	0.47 ± 0.11
$M_\star$	[$M_\odot$]	0.76	0.84	0.90
$v \sin i$	[km s^{-1}]	1	<1	2
$\log R'_{HK}$		–4.97	–4.95	–5.07
$P_{\rm rot}$	[days]	44 ± 5	26 ± 3	51 ± 5
Age	[Gyr]	~7.2	~4.4	~9.1

Notes. [(†)] Hipparcos catalogue (ESA 1997), Sousa et al. (2008). [(‡)] Hipparcos catalogue (ESA 1997), this work.

31 and 42 $M_\oplus$) without any analog in the solar system. We discuss the formation of the latter set of objects in the context of the core accretion formation model at the end of the paper. Such intermediate-mass planets are interesting because they provide observational constraints on the rate at which gas can be accreted by planets starting runaway gas accretion.

The paper is organized as follows. In Sect. 2 we discuss the host star properties. Radial velocity measurements and orbital solutions are presented in Sect. 3. In Sect. 4, we summarize our discoveries, and in Sect. 5 we discuss them.

2. Host star characteristics

The basic photometric and astrometric properties for the three host stars HD 85390 (HIP 48235), HD 90156 (HIP 50921), and HD 103197 (HIP 57931) were taken from the Hipparcos catalog (ESA 1997). Accurate spectroscopic stellar parameters and derived quantities for HD 85390 and HD 90156 were taken from the analysis of Sousa et al. (2008). Sousa et al. (2008) used high-quality, high signal-to-noise (S/N) HARPS spectra to obtain homogenous estimates of the spectroscopic stellar parameters of all 451 targets in the HARPS Guaranteed Time Observations (GTO) "high precision" sample, to which the two mentioned stars belong. HD 103197 is in contrast part of the lower RV precision "CORALIE extension" sample, see Naef et al. (2007). For this star, we stacked several individual spectra together to obtain a high S/N spectrum and repeated the analysis described in Sousa et al. (2008).

Individual HARPS spectra were used to derive the radial velocity RV, the bisector inverse slope of the cross-correlation function, the $v \sin i$ of the star, as well as the chromospheric activity index $\log R'_{HK}$, using a similar recipe as Santos et al. (2000). From the activity indicator we also derive an estimate of the stellar rotation period $P_{\rm rot}$ using the empirical Noyes et al. (1984) activity-rotation correlation. Approximate ages were obtained using the improved activity-rotation-age calibration of Mamajek & Hillenbrand (2008). These ages typically have errors of about 0.2 dex.

The basic properties of the four stars are summarized in Table 1. The stellar mass estimates from Sousa et al. (2008) typically have an error of 0.1 $M_\odot$.

2.1. HD 85390 (HIP 48235)

HD 85390 is a K1 dwarf in the southern hemisphere. The Hipparcos catalog (ESA 1997) lists a visual magnitude V = 8.54, a color index $B-V$ = 0.86, and an astrometric parallax π = 29.45 ± 0.84 mas, setting the star at a distance of 34 ± 1 pc from the Sun, a typical distance for planet-host stars in RV search programs. Its absolute magnitude is then estimated to be M_V = 5.89 mag. The spectral analysis of Sousa et al. (2008) yields the following physical parameters: an effective temperature $T_{\rm eff}$ = 5186±54 K, a surface gravity $\log g$ = 4.41±0.09, and a metallicity [Fe/H]= −0.07±0.03 dex. The star thus has a metallicity similar to the Sun. The derived mass is 0.76 $M_\odot$, and the luminosity is estimated from the absolute magnitude, the effective temperature, and the corresponding bolometric correction to be 0.43 $L_\odot$, hence less than half the solar luminosity. A low projected rotational velocity $v \sin i$ of about 1 km s^{-1} is derived from a calibration of the width of the cross-correlation function as described in Santos et al. (2002). With an activity indicator $\log R'_{HK}$ of –4.97, the star is among the non-active stars in our sample, and no large radial velocity jitter is expected. The detailed way we dealt with the stellar jitter is described in Sect. 3.1.

Several additional measurements of the properties of HD 85390 can be found in the literature that agree fairly well with the mentioned values. Gray et al. (2006) list a spectral type K1.5V, $T_{\rm eff}$ = 5069 K, $\log g$ = 4.48, [M/H] = −0.11, and $\log R'_{HK}$ of –5.06. Henry et al. (1996) measure a $\log R'_{HK}$ of –4.93. Minniti et al. (2009) classify the star as a K1 radial velocity stable star at a precision of about 5 m/s.

2.2. HD 90156 (HIP 50921)

According to the Hipparcos catalog (ESA 1997), HD 90156 is a fairly close G5V star with an astrometric parallax of π = 45.26 ± 0.75 mas with basic photometric properties of V = 6.92 and $B-V$ = 0.66. Sousa et al. (2008) use the HARPS spectra to derive $T_{\rm eff}$ = 5599 ± 12 K, $\log g$ = 4.48 ± 0.02, and a subsolar metallicity of [Fe/H] = −0.24 ± 0.01 dex, which is well known to play an important role in planet formation. Other derived quantities are $M_\star$ = 0.84 $M_\odot$ and L = 0.72 ± 0.01 $L_\odot$. The star has a low projected rotation velocity of less than 1 km s^{-1}, which is thus difficult to determine accurately, see Melo et al. (2001), and a low activity index of $\log R'_{HK}$ = −4.95.

The star has been studied by several other groups. It has, in particular, been spectroscopically analyzed by Valenti & Fischer (2005). By fitting synthetic spectra they find an effective temperature of 5626 ± 44 K and $\log g$ = 4.63 ± 0.06. This surface gravity is significantly greater than our value or their value calculated from isochrone interpolation ($\log g$ = 4.46), corresponding to a systematic discrepancy noted by the authors themselves. The mass derived from their spectroscopic gravities is, with 1.25 ± 0.17 $M_\odot$, correspondingly considerably higher than our value. On the other hand, is the mass they derive from interpolating isochrones with 0.90 ± 0.04 $M_\odot$ similar to our result. Valenti & Fischer (2005) also measure a subsolar metal content of [Fe/H]=−0.21 ± 0.03 and estimate the age of the star to be 7.8 Gyr.

The metal-poor nature of the star is further confirmed by Neves et al. (2009), who note that the star is a member of the thin disk, and by Gray et al. (2006) who find an [M/H] of –0.26. The latter authors also give $T_{\rm eff}$ = 5578 K, $\log g$ = 4.52, and $\log R'_{HK}$ = −4.96, which is comparable to our values. HD 90156 is listed in the catalog of suspected variable stars of Kukarkin et al. (1981) with an amplitude in V of 0.1 mag. The much more

accurate Hipparcos data does not, however, point to any significant variability.

2.3. HD 103197 (HIP 57931)

HD 103197 is classified in the Hipparcos catalog (ESA 1997) as K1Vp, with $V = 9.40$, $B - V = 0.86$, and $\pi = 20.27 \pm 1.47$ mas. Repeating the same spectroscopic analysis as described in Sousa et al. (2008) with stacked HARPS spectra leads to the following values: $T_{\rm eff} = 5303 \pm 58$ K, $\log g = 4.40 \pm 0.11$, and a supersolar metallicity of [Fe/H] $= 0.21 \pm 0.04$ dex. The derived mass and luminosity is 0.90 $M_\odot$ and 0.47 $L_\odot$. From the HARPS spectra, we also infer the following quantities: a projected rotational velocity of roughly $v \sin i \approx 2$ km s^{-1}, a low activity indicator $\log R'_{HK} = -5.07$, and an estimated $P_{\rm rot}$ of about 51 ± 5 days. This star is therefore very inactive.

For comparison, Jenkins et al. (2008) also find a low $\log R'_{HK} = -5.05$, but their [Fe/H] $= -0.12 \pm 0.04$ is clearly lower than our value.

3. Radial velocity measurements and orbital solutions

3.1. Jitter and error estimates

The quantified error of an individual radial velocity measurement includes photon noise, calibration, and instrumental drift uncertainty. Additional, unquantified errors that are not included in this number will originate from the intrinsic radial velocity variability of the star (jitter) due to granulation (Kjeldsen et al. 2005), magnetic activity, and pulsations (see Pepe & Lovis 2008, for an overview). This jitter can in principle be a serious threat to high-precision RV measurement at a level of 1 m/s (Wright 2005). On the other hand, there are now several stars in the HARPS high-precision program such as HD 69830 (Lovis et al. 2006) or HD 40307 (Mayor et al. 2009), for which residuals around the fit clearly below 1 m/s have been found, such as 0.64 m/s for HD 69830 (Lovis et al. 2006).

Neglecting the RV jitter in the total error estimate can have negative effects on the derivation of the uncertainties of the orbital parameters of the fits. Neglecting it has also the effect that measurements with a small quantified error (particularly high S/N, due to e.g. very good seeing to which HARPS is sensitive) get an inappropriately high weight in the fitting procedure, also causing misleading results.

Several authors have tried to derived empirical relations linking a star's radial velocity jitter to other quantities, such as $B - V$ or R'_{HK} (e.g. Saar et al. 1998; Wright et al. 2005). Concerning this work, all three stars presented here would fall in the class with the lowest derived median jitter of 3.5 m/s. The jitter of the stars presented here is, however, obviously significantly smaller, as can be seen by the fact that planets that induce a radial velocity semi-amplitude of that order are clearly detected in the data. This indicates that those older jitter estimates were clearly affected by instrumental and data reduction uncertainties.

We find from our HARPS measurements that for the typical stars in the high-precision program with insignificant evolution, a very low activity level ($\log R'_{HK} \leq -4.95$ like for the three stars in this work), a small interval in $B - V$ (usually 0.5–1.0, 0.66–0.86 in this paper), and a small $v \sin i$ (≤ 2 km s^{-1}), it is difficult to derive empirical relations like the ones mentioned before, which cover much larger domains of these quantities. For example, we do not see any obvious correlation between the minimal RV jitter and $\log R'_{HK}$ or $B - V$ among the stars with the properties mentioned for our sample. In a recent study, Isaacson & Fischer (2010) find at least qualitatively, very similar conclusions, in particular with a jitter level independent of activity indicators and below their instrumental and reduction precision (~1.6 m/s) for mid-to-late K dwarfs. For somewhat bluer stars, they derive slightly higher astrophysical jitter levels (~1.4 m/s), but still only a weak correlation with chromospheric activity.

It seems that in the high-precision HARPS data, the lower boundary of the minimal total rms is around 50 cm/s for stars with the parameters mentioned above and our current reduction pipeline. As gaining insight into the fundamental limiting factors for the radial velocity technique is an important task, we will present an in-depth analysis of the statistical properties of the sample regarding RV jitter in a dedicated forthcoming paper (Lovis et al., in prep.).

For the work presented here, we restrict ourselves to a pragmatic approach and compare the three stars with similar ones in the sample for which the jitter can be estimated in form of the rms of the residuals to the fitted orbits, σ(O−C). This number can, however, also contain additional contributions e.g. from undetected low mass planets. Both HD 85390 (K1V) and HD 103197 (K1V) are similar to HD 69830 (K0V) in terms of spectral type, effective temperature, and $\log R'_{HK}$, even though that HD 85390 is somewhat cooler than this star. As mentioned, for HD 69830 a σ(O−C) of 0.64 m/s was found in Lovis et al. (2006) for the later measurements. Since then, our calibration algorithm has been improved even more (Pepe & Lovis 2008). HD 90156 (G5V) is similar to HD 47186 (G5V) for which a total σ(O−C) of 0.91 m/s was found in Bouchy et al. (2009). From this we conclude that the typical levels of the unquantified errors are between 0.5 and 0.8 m/s, where the latter value has already been used in Pepe et al. (2007).

Following Saar et al. (1998) or Pepe et al. (2007), we then assume that we can quadratically add this estimated radial velocity jitter to the quantified error of each radial velocity measurement, using a constant value of either 0.5 or 0.8 m/s. This might not be completely justified, because depending on the physical nature of the variability source like magnetic cycles of the star (Santos et al. 2010), the jitter might instead be a red noise type and vary in time. Using such an additive procedure, we can, however, certainly mitigate the adverse effects of artificially high dynamics in the quantified (photonic) errors. We then search for an orbital solution in the data after adding these two values, and compare the impact on the best-fit parameters and their errors.

3.2. HD 85390: An intermediate-mass planet and a long-term drift

HD 85390 was monitored with HARPS for a time span of 6.5 years (2386 days), during which time 58 measurements were obtained. Except for the first six measurements, we always followed the observational strategy of using a fixed exposure time of 15 min in order to minimize the effects of stellar acoustic modes (Pepe & Lovis 2008). We nevertheless included the early, less accurate measurements to have a better constraint on the long-time drift present in the data. The spectra that were all obtained in ThAr simultaneous mode have a typical S/N at $\lambda = 550$ nm of 116 and a mean quantified error of the radial velocity (including photon noise, calibration, and instrumental drift uncertainty) of 0.62 m/s. Given the low chromospheric activity of the star, they should, however, induce a clearly smaller raw rms than the one found in the 58 measurements, which is 3.3 m/s (peak-to-peak 14.4 m/s), indicating instead the presence of a companion. To account for the unquantified errors (see

Sect. 3.1), we quadratically add an additional error of 0.5 resp. 0.8 m/s to all our measurements. Using either 0.5 m/s or 0.8 m/s only has a very minor influence on the orbital solutions: the derived quantities such as period P, mean longitude λ, eccentricity e, or velocity semi-amplitude K, agree to better than 2% for the two cases, much less than the error bars on these quantities. This is in good agreement with Wright (2005), who states that radial velocity jitter is more important in detecting extrasolar planets than in their characterization, and that the effects of including jitter in the noise estimation for the derived orbital parameters of the best fit is typically small, at least for a case like this one where the induced radial velocity signal is greater than the estimated jitter amplitude.

Radial velocity measurements as a function of Julian date (with 0.8 m/s of additional error) are shown as red dots in the top panel of Fig. 1. A long-term, linear drift overlaid by a higher frequency modulation with a period of about 800 d can be seen directly in the data. Of the latter, three phases are covered. The bottom panel of Fig. 1 shows the generalized Lomb Scargle periodogram (as described in Zechmeister & Kürster 2009) of the data. The peak at such a period is clear and has a very low FAP of less than 0.01%, as found by scrambling the data 10 000 times, which confirms the visual impression of a very clearly detected orbit. The FAPs are obtained by performing random permutations of the velocities, calculating the periodogram, recording the peak power for each trial, and finally comparing the power of the real signal to the peak power distribution of the permuted datasets.

We therefore fit the measurements with a linear drift and a Keplerian orbit, using a genetic algorithm (see below for a discussion of the nature of the drift). The resulting best fit and the residuals around it are also plotted in the top panel of Fig. 1. The phase-folded radial velocity curve of the planet candidate after removing the drift is shown in the middle panel of this figure. The reduced χ^2_r per degree of freedom is 1.52 (2.31 for an additional error of 0.5 m/s), and the weighted rms of the residuals around the solution σ(O−C) is 1.15 m/s (1.14 m/s for an additional error of 0.5 m/s), which is not much more than the mean total assumed error of the individual measurements. In the residuals, no additional significant periodic signals are found.

The somewhat higher σ(O−C) is also at least partially due to the mentioned six early measurements, which can be identified in Fig. 1 by their larger error bars. Excluding these six early radial velocities results in a very similar fit with a reduced χ^2_r = 1.10 (additional error of 80 cm/s) and reduces σ(O−C) to just 1.00 m/s.

The long-term signal is found to have slope of 1.15 ± 0.02 m/s yr^{-1}. The derived parameters for the Keplerian orbit imply a period P = 788 ± 25 d (corresponding to a semi-major axis a = 1.52 AU), a minimum mass of $M \sin i$ = 42.0 ± 3.6 $M_\oplus$ (2.44 M_{Jup}), and eccentricity e = 0.41 ± 0.12. The error intervals were computed for a 68% confidence level with 5000 Montecarlo iterations, where the actual measurements are replaced by a value drawn from a normal distribution around the nominal value with a standard deviation that is the same as the error bar on the point. These altered data sets are then fitted again to obtain the confidence intervals from the distribution of orbital elements one finds. The orbital elements are listed in Table 2. We checked that there is no correlation between bisector shape of the cross-correlation function and the radial velocity or the residuals of the Keplerian fit, providing strong support to the planetary interpretation of the RV signal.

HD 85390 is also part of the CORALIE planet search survey (Udry et al. 2000). Including the 19 measurements made with CORALIE expands the observed time base significantly to 11.3 years (4114 days), back to JD = 2 451 262, which could help to better constrain the long-term drift seen in the HARPS data. The radial velocity as a function of time for the two

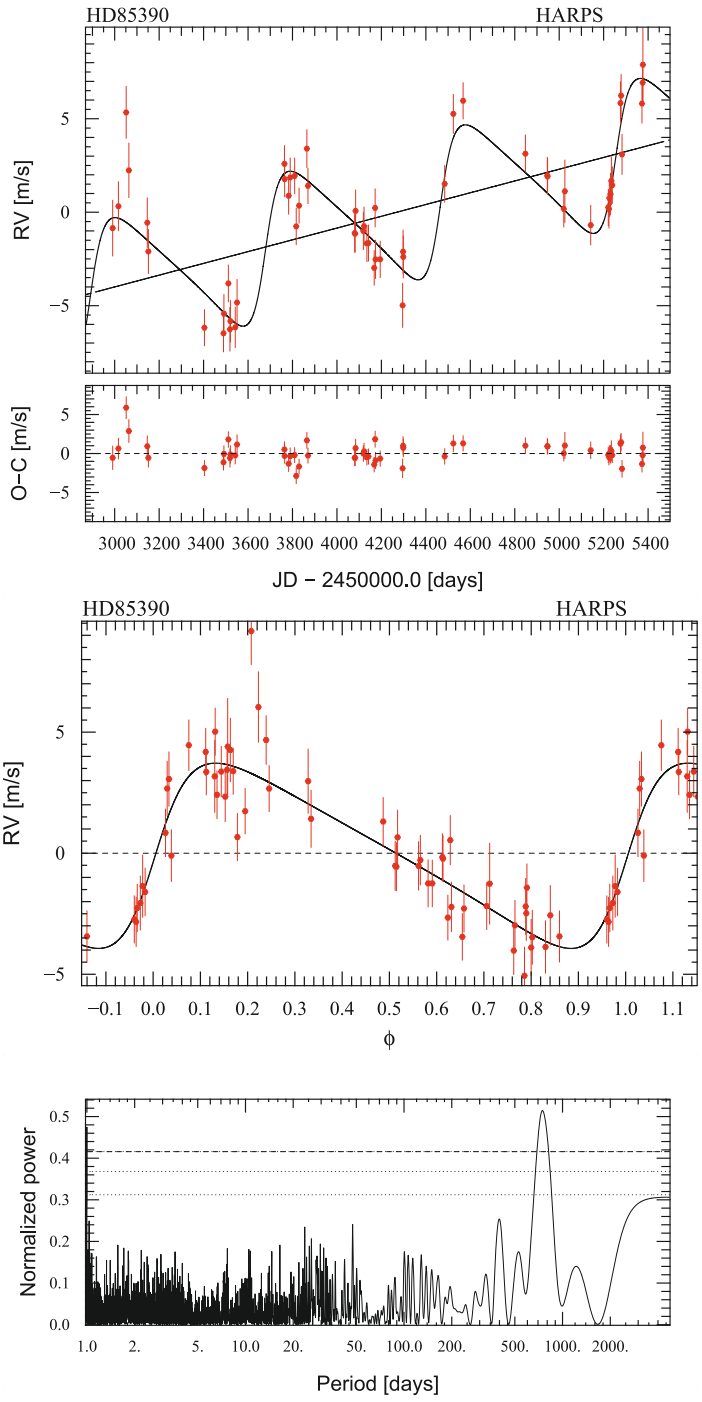

Fig. 1. Radial velocity measurements of HD 85390 as a function of Julian Date (*top*). The six earliest measurements have larger error bars. The best solution with a linear drift plus one Keplerian orbit is also displayed as the residuals to this model. The *middle panel* shows the radial velocity as a function of the orbital phase for HD 85390 b, with the effect of the drift removed. The *bottom panel* shows the generalized Lomb Scargle periodogram of the observations. The peak at a period of about 800 days is very prominent, and has a false alarm probability (FAP) of much less than 0.1%. The three horizontal lines indicate FAPs of 0.1, 1, and 10% from *top to bottom*.

Table 2. Orbital and physical parameters of the 1-planet plus linear drift solution of the HARPS data for the objects around HD 85390.

Parameters		HD 85390 b
P	[days]	788 ± 25
$\lambda^{\dagger}$	[deg]	177 ± 25
e		0.41 ± 0.12
ω	[deg]	−94 ± 23
K	[m/s]	3.82 ± 0.33
V	[km s^{-1}]	33.0853 ± 0.0004
slope	[m/s yr^{-1}]	1.15 ± 0.02
$f(m)$	[10^{-9} $M_{\odot}$]	0.0035 ± 0.0009
$M \sin i$	[$M_{\oplus}$]	42.0 ± 3.6
a	[AU]	1.52 ± 0.04
$N_{\rm meas}$		58
span	[years]	6.5
σ(O−C)	[m/s]	1.15
χ^2_r		1.52

Notes. $^{(\dagger)}$ Mean longitude at the barycenter of the observations at BJD 54269.3584.

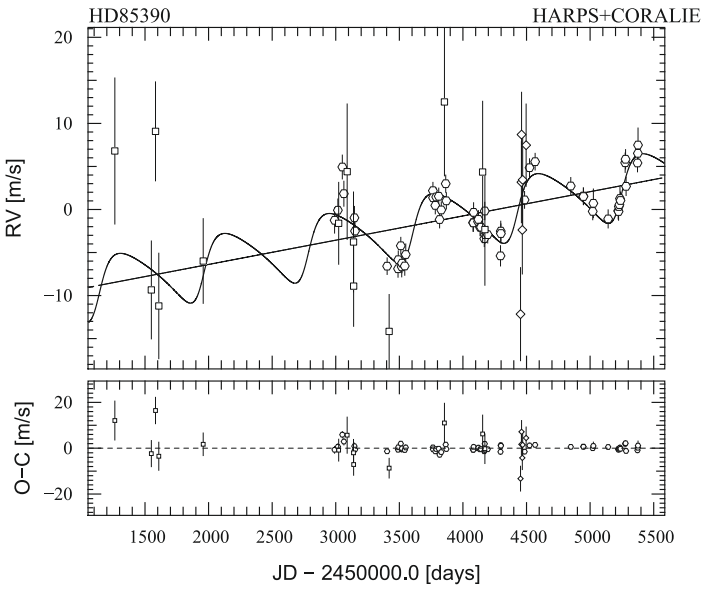

Fig. 2. Radial velocity measurements of HD 85390 as a function of Julian Date for the combined data set of CORALIE (squares for measurement before its upgrade in June 2007 and diamonds after this moment) and HARPS (circles), together with one Keplerian plus linear drift fit (solid line). The small panel shows the residuals around the fit.

instruments is shown in Fig. 2. It is found that at the level of precision of CORALIE (about 6.5 m/s for this target), the star is stable, i.e. the ratio of the rms of all the velocity measurement and the mean error of one velocity measurement is about unity. Repeating the fitting process with the combined data set leads to a solution for the Keplerian orbit that agrees within the error bars with the solution without the CORALIE data, namely $P = 821 \pm 20$ d, $e = 0.34 \pm 0.10$, and $M \sin i = 42.3 \pm 3.5\, M_{\oplus}$, with a χ^2_r of 1.59 for additional jitter of 0.8 m/s in the HARPS measurement. The linear component of the drift is now 1.03 ± 0.02 m/s yr^{-1}. From that we can exclude the presence of a massive outer companion with a period less than about 10 years.

In the nominal model for the orbital solution, we have assumed a Keplerian orbit plus a linear drift. One wonders if we could significantly improve the fit by allowing for a quadratic component in the drift, as one could tentatively infer from two early CORALIE measurements lying 12 resp. 16 m/s above the linear fit.

This could be indicating the presence of a body that might be interesting for direct imaging searches. To explore this significance, we fitted the combined dataset of HARPS and CORALIE, which is more relevant in this context as it constrains the long time behavior better also with a Keplerian plus a quadratic drift. The orbital solution for the Keplerian orbit then corresponds to a companion with properties that again agree within the error bars with the solution shown in Table 2. This is because the HARPS measurements alone constrain this orbit. The reduced χ^2_r for the combined data are now 1.47 for an additional errors of 0.8 m/s, i.e. somewhat less than for the linear model with one degree of freedom less. We then used an F-test as in Pourbaix & Arenou (2001) to get the statistical probability that the improvement due to the quadratic model is significant. We find a probability of 98.7%, corresponding to about 2.5 sigma. The main assumption behind the F-Test is, however, that the model is linear and that the error distribution is Gaussian, neither of which is strictly fulfilled, therefore this number must be regarded with caution. Because the orbital solution of HD 85390 b itself is not significantly affected by the choice, we prefer to stick to the simpler linear model for the moment and conclude that to further constrain the nature of the long-term drift, more high-precision observations with HARPS are needed.

Long-term, small amplitude signals could also in principle be due to magnetic cycles of the host star. While we cannot absolutely exclude this possibility, we think that it is unlikely in the present case for the following reasons. First, during the observed time span, $\log R'_{HK}$ decreases linearly from about −4.93 to −5.00. Thus, the change of $\log R'_{HK}$ and the long-term drift in the radial velocity are clearly anti-correlated. This is the contrary of what is expected, as in active zones, convection tends to be inhibited, reducing the convective blue shift, so that a shift of the radial velocity into the red should occur (Santos et al. 2010). Second, the change of $\log R'_{HK}$, about 0.07 dex is less than the value of about 0.1 dex where we start to see clear correlations of the activity level and the radial velocity in the HARPS database (Lovis et al., in prep.). Third, the amplitude of the drift is large (about 8 m/s), much more than expected for the small change in $\log R'_{HK}$ for a K dwarf.

3.3. HD 90156: A warm Neptune analog

Since the mentioned change in strategy to minimize stellar noise (fixed exposure times of 15 min), we have gathered 66 radial velocities in ThAr simultaneous mode during a time period of 1614 days (4.4 years). HD 90156 is a bright star ($V = 6.92$), therefore the measurements have a high mean S/N of 246 at 550 nm, with variations of the S/N between 121 and 342, mostly depending on seeing conditions. The derived mean quantified error (photon noise, calibration, and drift uncertainty) is 0.41 m/s. The observed raw rms for the 66 measurements is 2.6 m/s, again more than expected for the low stellar activity level. As before, we add quadratically an additional error of either 0.5 or 0.8 m/s to all measurements and check for the consequences.

A periodogram of the data displayed in the top panel of Fig. 3 shows a very strong peak at a period of about 50 days with an FAP of much less than 0.1% as obtained by executing 10 000 data scrambling experiments. A number of aliases can also be seen. A one-Keplerian fit assuming an additional RV error of 0.8 m/s quickly converges on a solution with a $M \sin i = 17.98 \pm 1.46\, M_{\oplus}$ planet on an orbit with a period of

Table 3. Orbital and physical parameter of the 1-planet Keplerian solution for the planet around HD 90156.

Parameters		HD 90156 b
P	[days]	49.77 ± 0.07
$\lambda^{\dagger}$	[deg]	91 ± 15
e		0.31 ± 0.10
ω	[deg]	113 ± 18
K	[m/s]	3.69 ± 0.25
V	[km s^{-1}]	27.0273 ± 0.0003
$f(m)$	[10^{-9} $M_{\odot}$]	0.00022 ± 0.00005
$M \sin i$	[$M_{\oplus}$]	17.98 ± 1.46
a	[AU]	0.250 ± 0.004
$N_{\rm meas}$		66
span	[years]	4.4
σ(O−C)	[m/s]	1.23
χ^2_r		2.03

Notes. $^{(\dagger)}$ The mean longitude λ is given at the barycenter of the observations, at JDB 54772.0784.

49.77 ± 0.07 days and an eccentricity of 0.31 ± 0.10. This solution and the measurements are shown in the lower two panels of Fig. 3. The reduced χ^2_r is 2.03, and the σ(O−C) is 1.23 m/s (see Table 3). The mentioned period corresponds to a semi-major axis of 0.25 AU, and the projected mass is very close to the mass of Neptune (1.05 $M_{\oplus}$), making this planet a warm Neptune analog. We checked that there is no correlation between the bisector shape of the cross-correlation and the radial velocity or the residuals around the Keplerian fit. Assuming an additional error of 0.5 instead of 0.8 m/s leads to virtually identical fit parameters with relative differences of less than 3%. The reduced χ^2_r increases to 3.91, indicating that we now underestimate the unquantified errors in the measurements. We note the subsolar metallicity of the parent star, so that HD 90156 b is another example of a Neptunian planet not following the "metallicity effect" seen for giant planets, as discussed for example in Sousa et al. (2008). It is also an example of a warm low-mass planet that does not show the same strong pile-up behavior at about 0.04 AU, as higher mass Hot Jupiters do (Udry & Santos 2007).

In a periodogram of the residuals around the one planet fit, there is a signal at a period of about 14 days. With an FAP of 16%, we can however not yet conclude anything about its origin. We do hope to soon be able to either confirm or reject this signal by additional observations.

3.4. HD 103197: An intermediate-mass planet

We have gathered 58 high quality radial velocity measurement of HD 103197 over a time period of 6.12 years. They are shown in the top panel of Fig. 4. The mean exposure time for this star was shorter than for the other two, since it does not belong to the high-precision sample and is close to 5 min, which should still be just sufficient to average out the most important stellar oscillation period for this type of star (cf. Pepe & Lovis, 2008). Corresponding to the smaller exposure time, the spectra have a lower typical S/N at 550 nm, namely between 33 and 107 with a mean of 59. The error on a single radial velocity measurement, which includes photon noise, calibration, and spectrograph drift uncertainty, varies between 0.7 and 2.3 m/s, with a mean of 1.1 m/s. The observed raw rms of the radial velocities is clearly larger with 3.95 m/s, and it indicates the presence of a companion. As before, we quadratically add additional errors of 0.8 and 0.5 m/s. For this star, no ThAr simultaneous reference

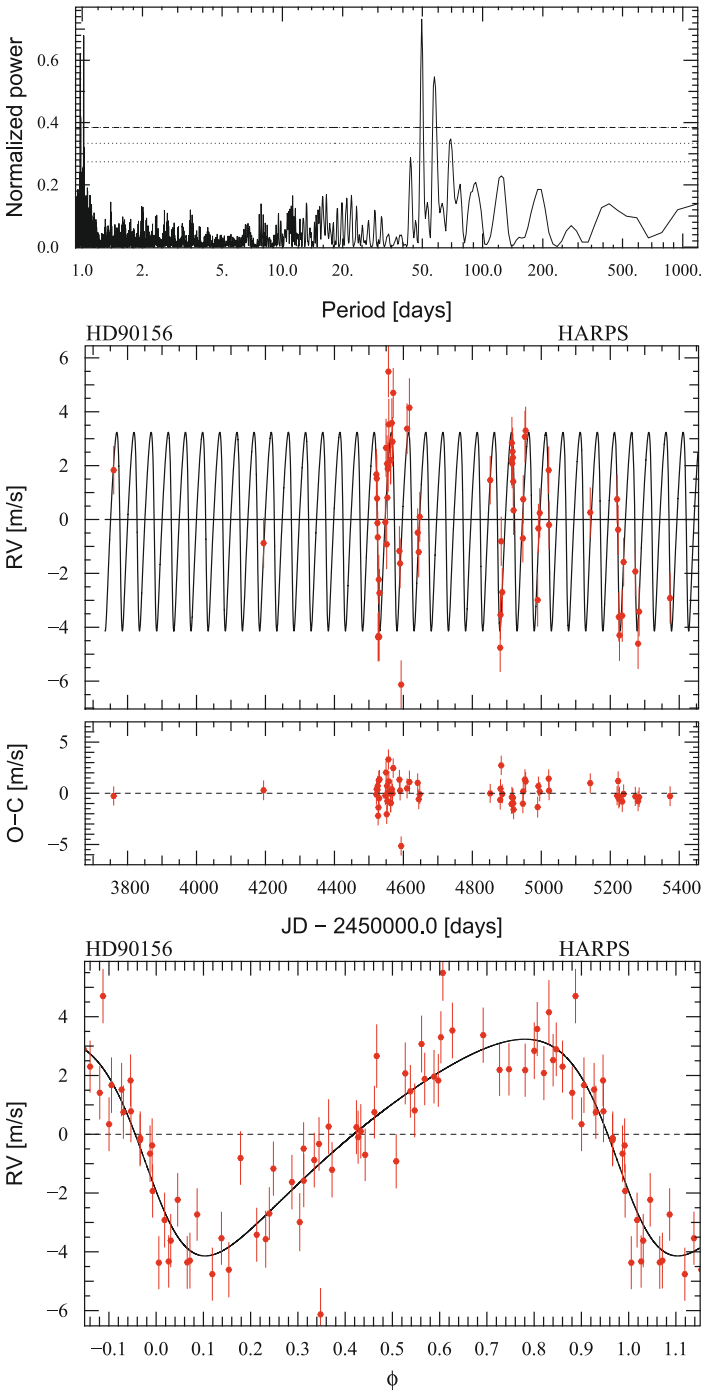

Fig. 3. *Top panel*: generalized Lomb Scargle periodogram of the radial velocity measurements of HD 90156. An FAP of 0.1% is indicated by the dashed-dotted line. The peak at about 50 days is very clear and has an FAP far below this value. *Middle panel*: radial velocities and residuals as a function of Julian Date and (*bottom panel*) as a function of orbital phase for the one-planet Keplerian fit (P = 49.8 days).

mode was usually used, which is, however, unproblematic given the very small nightly drift of the instrument and the fact that we mix observations with and without ThAr during one night.

A periodogram of our radial velocity data shows a very strong peak at a period of about 48 days, as can be seen in the top panel of Fig. 4, where horizontal lines again indicate FAPs of 10^{-1}, 10^{-2}, and 10^{-3} from bottom to top. Fitting the data with one Keplerian orbit leads to a solution with an insignificant

eccentricity (0.04 ± 0.05) so that we fix it to zero, leaving us with four free parameters.

The following solution is then found for the companion, assuming an additional radial velocity jitter of 0.8 m/s: an orbital period of 47.84 ± 0.03 days, a mean longitude $\lambda = 151 \pm 3$ deg at JDB 54846.0994 and $K = 5.9 \pm 0.3$ m/s, implying a minimum mass $M \sin i = 31.2 \pm 2.0\, M_\oplus$, and a semi-major axis $a = 0.25$ AU. The mass corresponds to 1.8 M_{Sat}. The fit has a reduced χ^2_r of 1.02 and σ(O−C) = 1.40 m/s, which corresponds well to the total assumed mean error of the individual measurements. As for the two previously discussed stars, using an additional jitter of 0.5 m/s instead of 0.8 m/s has only a very minor influence on the fit, and results in a $\chi^2_r = 1.18$. The middle and lower panels of Fig. 4 show the radial velocities and the fit as a function of time and phase-folded, as well as the residuals around the fit. The orbital elements for the Keplerian fit with $e = 0$ are given in Table 4. The errors were again derived from 5000 Monte Carlo simulations.

The orbital period is similar to the rotation period of the star P_{rot}, which we estimate to be 51 ± 5 days. We did, however, check for periodicity in the bisector shape at such a period and for a significant correlation of the velocity or the residual and the bisector shape, finding no such signs. We finally looked at the periodogram of the residual around the fit and discovered no additional significant signal.

4. Summary

We have reported in this paper the discovery of three extrasolar planet candidates discovered with the HARPS Echelle spectrograph mounted on the 3.6-m ESO telescope located at La Silla Observatory. HD 85390 b is an intermediate-mass planet ($M \sin i = 42.0\, M_\oplus$) on an orbit with a semi-major axis of 1.5 AU. A drift indicates there is an additional outer companion, but we cannot currently determine its nature with our data. HD 90156 b is a warm Neptune analog ($M \sin i = 1.05\, M_{\mathrm{Sat}}$, $a = 0.25$ AU). HD 103197 b is another intermediate-mass planet ($M \sin i = 31.2\, M_\oplus$). Its semi-major axis is 0.25 AU.

5. Discussion: formation of intermediate-mass planets

By intermediate-mass planets we here refer to planets with a mass greater than Neptune's, but less than Saturn's. They therefore fall in the significant mass gap of a factor 5 between Uranus ($17.2\, M_\oplus$) and Saturn ($95.2\, M_\oplus$), which corresponds to a large difference in internal composition, too: Uranus and Neptune are ice giants that mainly consist of heavy elements (iron, rocks, and ices) and only about 5–15% in mass of hydrogen and helium (e.g. Figueira et al. 2009). Saturn and Jupiter are, in contrast, gas giants with only a small fraction of heavy elements. Instead, their massive gas envelopes account for most of the mass, for about 67 to 80% for Saturn and 87 to 97% for Jupiter (Guillot 1999).

This difference in mass and composition is in turn understood in theoretical formation models based on the core accretion paradigm as the consequence of an important difference in the formation history of these two groups of planets. Jupiter and Saturn are thought to have undergone a phase of rapid "runaway" gas accretion, during which they accreted their large gaseous envelopes on a relatively short timescale, whereas the ice giants never went through this phase (Pollack et al. 1996).

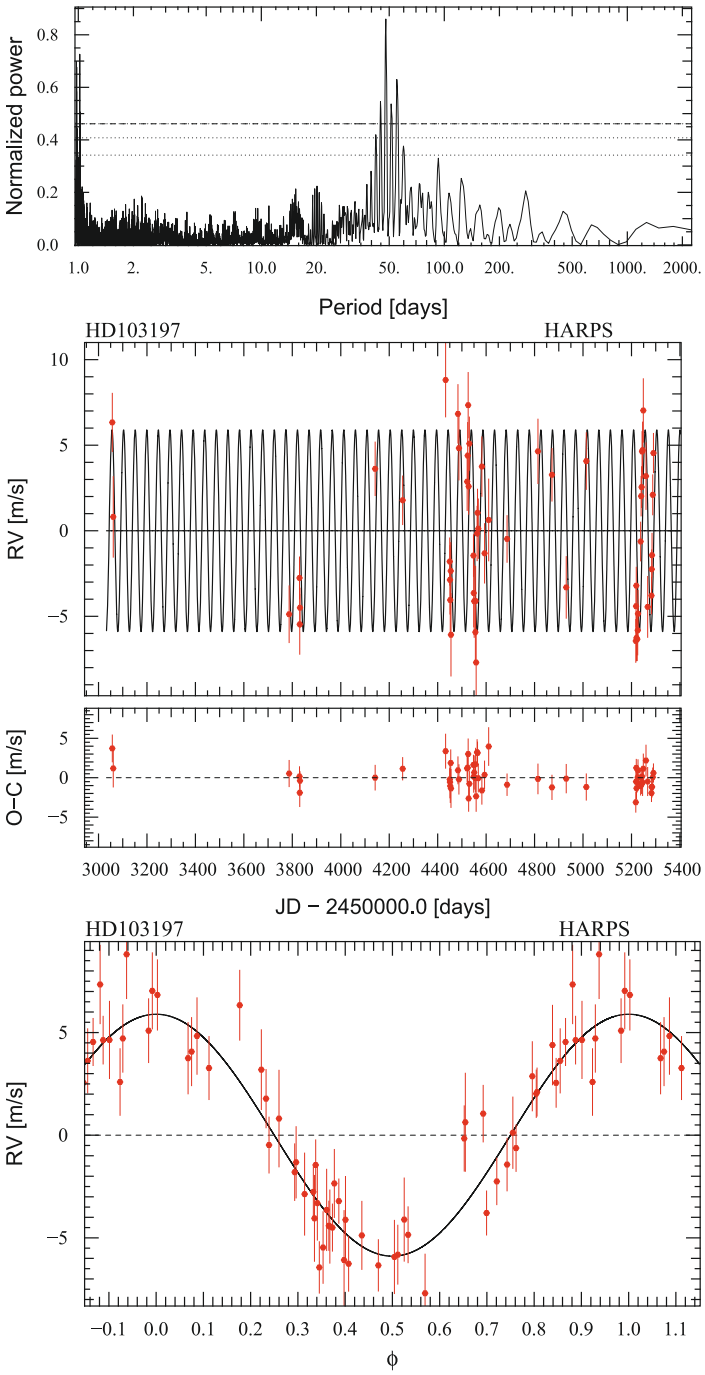

Fig. 4. *Top panel*: generalized Lomb Scargle periodogram of the 58 radial velocity measurements of HD 103197. The *middle and bottom panels* show the radial velocity and the residuals as a function of Julian Date, and as a function of orbital phase, together with the orbital solution given in Table 4.

If the transformation phase from a Neptunian mass to a Jovian mass is very short compared to the lifetime of the protoplanetary disk, i.e. if the gas accretion rate onto the planet is very high, then it is very unlikely that the protoplanetary disk disappears just during this phase, which would obviously terminate the gas accretion and leave the planet at some intermediate mass. We thus see that in this scenario, the absence of a planet with a mass between Uranus and Saturn is not a surprise, but rather an expected outcome (Ida & Lin 2004).

Table 4. Orbital and physical parameter of the 1-planet Keplerian solution for the companion around HD 103197, with the planet's eccentricity fixed to zero.

Parameters		HD 103197 b
P	[days]	47.84 ± 0.03
$\lambda^{\dagger}$	[deg]	151 ± 3
e		0.0 (fixed)
ω	[deg]	0.0 (fixed)
K	[m/s]	5.9 ± 0.3
V	[km s^{-1}]	−4.3282 ± 0.0002
$f(m)$	[10^{-9} $M_{\odot}$]	0.0010 ± 0.0002
$M \sin i$	[$M_{\oplus}$]	31.2 ± 2.0
a	[AU]	0.249 ± 0.004
$N_{\rm meas}$		58
span	[years]	6.12
σ(O−C)	[m/s]	1.4
χ^2_r		1.02

Notes. [(†)] The epoch of λ is JDB 54846.0994.

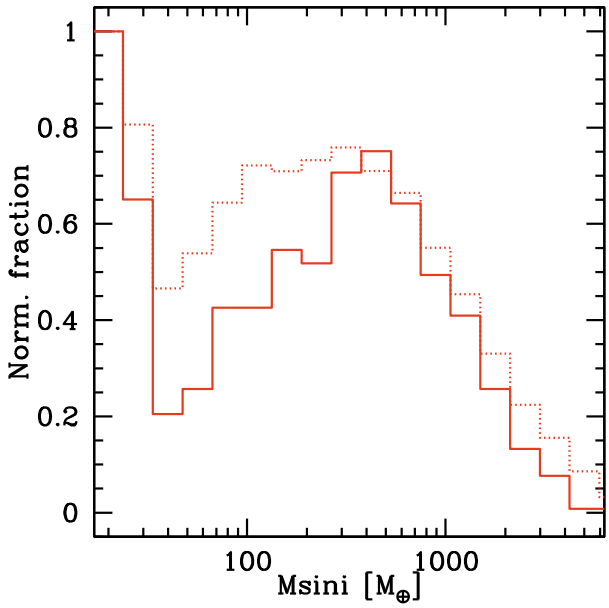

Fig. 5. Theoretical mass distribution from Neptunian to Jovian mass planets obtained from population synthesis calculations. The solid line shows a population where the planetary gas accretion rate was only limited by the disk accretion rate if the planet has a mass higher than the local gas isolation mass. For the dotted line, the limit was always used. Both distributions were normalized to unity at the first bin at about 20 Earth masses.

One can therefore say that the higher (smaller) the gas accretion rate in runaway, the smaller (higher) the expected relative frequency of intermediate mass planets compared to giant planets. This correlation will manifest itself in the observed detection rate of intermediate-mass extrasolar planets. Detections made over the last few years, in particular with the HARPS instrument, indicate a possible minimum of the planetary mass function at about 30–40 $M_{\oplus}$ (e.g. Bouchy et al. 2009). Such a minimum (if further confirmed) would be a very important observational finding, as it cannot be explained by an observational bias. This is because the lower mass Neptunian and super-Earth planets are more difficult to detect than intermediate-mass planets. It is interesting to note that a relative paucity of intermediate-mass planets also seems to exist in transit searches (Hartman et al. 2009).

Several physical effects influence the runaway gas accretion rate (Lubow et al. 1999; Ida & Lin 2004; Mordasini et al. 2009a; Lissauer et al. 2009). Thermal pressure in the planetary envelope at lower planetary masses, the global evolution (dissipation) of the protoplanetary disk that reduces the amount of matter available for the planet, the rate of mass transport due to viscosity within the disk towards the planet, as well as local phenomena like the formation of a gap.

While several planetary population synthesis simulations built on the core accretion paradigm share the feature of predicting some depletion of intermediate-mass planets relative to other planet types, they attribute in their underlying formation models (cf. Alibert et al. 2005) distinct importance to the various effects mentioned above, so that there are clear differences in the degree of depletion: from an almost complete absence of such planets between 0.1–1 AU (Miguel & Brunini 2008, 2009), over a significant depletion (Ida & Lin 2004, 2008a,b), to a rather moderate one (about a factor 2–3 relative to Jovian planets) in Mordasini et al. (2009a,b).

The reason for the difference between these last two models was discussed in detail in Mordasini et al. (2009a). It is related to different assumptions about the amount of gas present in the vicinity of the planet, as discussed next. Here we illustrate this in Fig. 5, which shows the theoretically obtained mass distribution from Neptunian to Jovian planets using two different assumptions for the gas accretion rate in runaway. Other settings are similar to those in Mordasini et al. (2009a). Only planets with a period less than 5 years are shown, which are detectable for an RV instrument of 1 m/s precision, similar to HARPS.

In one simulation (solid line), the gas accretion rate of the planet is limited by the accretion rate in the disk only if the mass of the planet is higher than the local gas isolation mass, calculated with the undisturbed gas surface density. This is similar to the criterion used by Ida & Lin (2004). It means that for masses between roughly 30 up to ∼100 $M_{\oplus}$ i.e. before the gas isolation mass is reached, high gas accretion rates of up to roughly 10^{-2} $M_{\oplus}$/yr can occur, so that the transformation from a Neptunian to a Jovian planet only takes about 10^4 years, much fewer than typical disk lifetimes. The underlying assumption here is that gas already inside the planet's Hill sphere can be accreted independently of the inflow from farther away in the disk. This inflow is in turn limited by the disk viscosity.

In the other simulation (dotted line), the planetary gas accretion rate is limited by the accretion rate in the disk as soon as runaway starts. As cores reach a mass high enough to trigger gas runaway accretion at a moment typically not much before the disk goes away (it is recalled that around about 90% of FGK stars, there are no giant planets), the accretion rate in the disk has usually already fallen to quite low values at this moment, of a few 10^{-4} to 10^{-3} $M_{\oplus}$/yr. This means that the transformation from a Neptunian to a Jovian planet now takes several 10^5 years, which is not much shorter than the remaining disk life time. The underlying assumption here is that due to gap formation, the mass directly available to the planet is in fact small, in particular less than the gas isolation mass calculated above, as (beginning) gap formation reduces the gas surface density around the planet. This corresponds to the setting in Mordasini et al. (2009a).

The plot shows that the two different settings have a strong effect on the frequency of intermediate-mass planets. They are, in the first model, clearly less frequent than in the second one,

with a factor of two difference for $M \approx 40\,M_\oplus$. Thus, the frequency of intermediate-mass planets can be used to directly improve our theoretical understanding of the accretion process.

Bodies with masses of up to several ten Earth masses can in principle also form after the dissipation of the gas disk if enough solids are available in situ, which is in particular the case at longer distances beyond the ice line. Such bodies would then essentially be gas free. At the rather short orbital distances of HD 85390 b and HD 103197 b (1.5 and 0.25 AU, respectively) for realistic solid disk masses, such a formation scenario seems however unlikely: The two planets are larger than what can be formed by this process at their current distances (Ida & Lin 2004), considering the host star's metallicities.

The two intermediate-mass planets were therefore very probably formed while the gas disk was still present. In this case, the mass of a planet core cannot grow to arbitrarily high values without runaway gas accretion setting in. The real masses of HD 85390 b and HD 103197 b, which are on the statistical mean a factor $4/\pi$ higher than the projected ones, are probably higher than the mass at which this process starts (although not by a large factor, especially for HD 103197 b, and the specific value depends on e.g. the unknown core accretion rate, see Papaloizou & Terquem 1999). These two planets are therefore probably examples where gas runaway started, but only shortly before the gas disk disappeared, so that only low quantities of gas were still available to accrete, and that the gas accretion rate was low. It is found that synthetic planets with a mass and orbital distance similar to HD 85390 b ($M \sin i = 42\,M_\oplus$) consist of typically about 40% hydrogen and helium in mass. The scatter around this value is quite large, reflecting different disk properties, and ranges from still clearly solid dominated planets (~10% gas) to small gas giants (~70% gas). For the less massive HD 103197 b ($M \sin i = 31.2\,M_\oplus$) the typical value is about 30% of gas, with a scatter around this value of about 15%. We conclude that these two exoplanets thus probably have not only a mass, but also an internal composition between Neptunian and Jovian planets.

From this discussion we see that it is important to observationally infer relative frequencies of planetary types between 20 to 100 $M_\oplus$ to better understand the runaway phase. This will finally enable us to construct better formation models. In the ideal case, the planets should be transiting their host star, but still be located so far away from it that significant evaporation can be ruled out, so that the primordial composition can be studied.

Acknowledgements. We thank the different observers from other HARPS GTO subprograms, who have also measured the stars presented here, and the observers of HD 85390 at CORALIE. We thank Xavier Dumusque for helpful input. We thank the Swiss National Research Foundation (FNRS) for its continuous support. Christoph Mordasini acknowledges the financial support as a fellow of the Alexander von Humboldt foundation. Nuno C. Santos would like to acknowledge the support by the European Research Council/European Community under the FP7 through a Starting Grant, as well as from Fundação para a Ciência e a Tecnologia (FCT), Portugal, through program Ciência 2007, and in the form of grants reference PTDC/CTE-AST/098528/2008 and PTDC/CTE-AST/098604/2008. We thank an anonymous referee for helpful comments.

References

Alibert, Y., Mordasini, C., Benz, W., & Winisdoerffer, C. 2005, A&A, 434, 343
Boss, A. 1995, Science, 267, 360
Bouchy, F., Mayor, M., Lovis, C., et al. 2009, A&A, 496, 527
Figueira, P., Pont, F., Mordasini, C., et al. 2009, A&A, 493, 671
Fischer, D. A., & Valenti, J. 2005, ApJ, 622, 1102.
Goldreich, P., & Tremaine, S. 1980, ApJ, 241, 425
Gray, R. O., Corbally, C. J., Garrison, R. F., et al. 2006, AJ, 132, 161
Guillot, T. 1999, Science, 286, 72.
Hartman, J. D., Bakos, G. Á., Torres, G., et al. 2009, ApJ, 706, 785
Henry, T. J., Soderblom, D. R., Donahue, R. A., & Baliunas, S. L. 1996, AJ, 111, 439
Ida, S., & Lin, D. N. C. 2004, ApJ, 604, 388
Ida, S., & Lin, D. N. C. 2008a, ApJ, 685, 584
Ida, S., & Lin, D. N. C. 2008b, ApJ, 673, 487
Isaacson, H., & Fischer, D. A. 2010, ApJ, 725, 875
Jenkins, J. S., Jones, H. R. A., Pavlenko, Y., et al. 2008, A&A, 485, 571
Kjeldsen, H., Bedding, T. R., Butler, R. P., et al. 2005, ApJ, 635, 1281
Kukarkin, B. V., Kholopov, P. N., Artiukhina, N. M., et al. 1981, Catalogue of suspected variable stars. Moscow, Acad. of Sciences, USSR Sternberg
Lissauer, J. J., Hubickyj, O., D'Angelo, G., & Bodenheimer, P. 2009, Icarus, 199, 338
Lovis, C., Mayor, M., Pepe, F., et al. 2006, Nature, 441, 305
Lovis, C., Mayor, M., Bouchy, F., et al. 2009, IAU Symp., 253, 502
Lubow, S. H., Seibert, M., & Artymowicz, P. 1999, ApJ, 526, 1001
Mamajek, E. E., & Hillenbrand, L. A. 2008, ApJ, 687, 1264
Mayor, M., & Queloz, D. 1995, Nature, 378, 355
Mayor, M., Bonfils, X., Forveille, T., et al. 2009, A&A, 507, 487
Melo, C. H. F., Pasquini, L., & De Medeiros, J. R. 2001, A&A, 375, 851
Miguel, Y., & Brunini, A. 2008, MNRAS, 387, 463
Miguel, Y., & Brunini, A. 2009, MNRAS, 392, 391
Minniti, D., Butler, R. P., López-Morales, M., et al. 2009, ApJ, 693, 1424
Mordasini, C., Alibert, Y., & Benz, W. 2009a, A&A, 501, 1139
Mordasini, C., Alibert, Y., Benz, W., & Naef, D. 2009b, A&A, 501, 1161
Naef, D., Mayor, M., Benz, W., et al. 2007, A&A, 470, 721
Neves, V., Santos, N. C., Sousa, S. G., Correia, A. C. M., & Israelian, G. 2009, A&A, 497, 563
Noyes, R. W., Hartmann, L. W., Baliunas, S. L., Duncan, D. K., & Vaughan, A. H. 1984, ApJ, 279, 763
Papaloizou, J. C. B., & Terquem, C. 1999, ApJ, 521, 823
Pepe, F., Mayor, M., Rupprecht, G., et al. 2002, The Messenger, 110, 9
Pepe, F., Correia, A. C. M., Mayor, M., et al. 2007, A&A, 462, 769
Pepe, F. A., & Lovis, C. 2008, Phys. Scrip. Vol. T, 130, 014007
Pollack, J. B., Hubickyj, O., Bodenheimer, P., et al. 1996, Icarus, 124, 62
Pourbaix, D., & Arenou, F. 2001, A&A, 372, 935
Saar, S. H., Butler, R. P., & Marcy, G. W. 1998, ApJ, 498, L153
Santos, N. C., Mayor, M., Naef, D., et al. 2000, A&A, 361, 265
Santos, N. C., Israelian, G., & Mayor, M. 2001, A&A, 373, 1019
Santos, N. C., Mayor, M., Naef, D., et al. 2002, A&A, 392, 215
Santos, N. C., Bouchy, F., Mayor, M., et al. 2004, A&A, 426, L19
Santos, N. C., Gomes da Silva, J., Lovis, C., & Melo, C. 2010, A&A, 511, A54
Sousa, S. G., Santos, N. C., Mayor, M., et al. 2008, A&A, 487, 373
Udry, S., & Santos, N. C. 2007, ARA&A, 45, 397
Udry, S., Mayor, M., D. Naef, D., et al. 2000, A&A, 356, 590
Valenti, J. A., & Fischer, D. A. 2005, ApJS, 159, 141
Wright, J. T. 2005, PASP, 117, 657
Zechmeister, M., & Kürster, M. 2009, A&A, 496, 577